

Safety and function of a new pre-vascularized bioartificial pancreas in an allogeneic rat model

Journal of Tissue Engineering
Volume 11: 1–16
© The Author(s) 2020
Article reuse guidelines:
sagepub.com/journals-permissions
DOI: 10.1177/2041731420924818
journals.sagepub.com/home/tej



Jordan Magisson¹, Aladin Sassi¹, Daela Xhema²,
Aram Kobalyan¹, Pierre Gianello², Brice Mourer³,
Nguyen Tran³, Charles-Thibault Burcez¹, Richard Bou Aoun¹
and Séverine Sigrist¹

Abstract

Cell encapsulation could overcome limitations of free islets transplantation but is currently limited by inefficient cells immune protection and hypoxia. As a response to these challenges, we tested in vitro and in vivo the safety and efficacy of a new macroencapsulation device named MailPan[®]. Membranes of MailPan[®] device were tested in vitro in static conditions. Its bio-integration and level of oxygenation was assessed after implantation in non-diabetic rats. Immune protection properties were also assessed in rat with injection in the device of allogeneic islets with incompatible Major Histocompatibility Complex. Finally, function was assessed in diabetic rats with a Beta cell line injected in MailPan[®]. In vitro, membranes of the device showed high permeability to glucose, insulin, and rejected IgG. In rat, the device displayed good bio-integration, efficient vascularization, and satisfactory oxygenation (>5%), while positron emission tomography (PET)-scan and angiography also highlighted rapid exchanges between blood circulation and the MailPan[®]. The device showed its immune protection properties by preventing formation, by the rat recipient, of antibodies against encapsulated allogeneic islets. Injection of a rat beta cell line into the device normalized fasting glycemia of diabetic rat with retrieval of viable cell clusters after 2 months. These data suggest that MailPan[®] constitutes a promising encapsulation device for widespread use of cell therapy for type 1 diabetes.

Keywords

Cell encapsulation, diabetes, medical device, membranes, pre-vascularization

Received: 17 February 2020; accepted: 18 April 2020

Introduction

Since 30 years now,¹ clinical islet transplantation^{2,3} demonstrated its feasibility and efficacy around the world. However, the widespread use of this therapy is first limited by the need for immunosuppressive drugs that might lead to significant side-effects, resulting in a favorable benefit–risk balance only for adults with brittle diabetes⁴ with recurrent severe hypoglycemic events.⁵ The other major limitation is related to organ shortage combined to low islet isolation yield, which results in a donor: recipient ratio of 2:1 to 4:1.^{6–8} For this reason, extensive work is ongoing to test alternative cell sources such as stem cell–derived beta cells^{9,10} or porcine islets.¹¹ However, such cells may have to be contained in a device, primarily due to potential Porcine Endogenous Retrovirus (PERV)

transmission to the recipient by pig islets^{12,13} and risk of teratoma formation by engineered stem cells.^{14–16}

In that sense, the concept of immune isolation of insulin-secreting cells emerged more than 30 years ago.¹⁷ It consists of encapsulating cells with a physical barrier to protect them from the immune system of the recipient and protect the recipient from the foreign cells. This strategy,

¹Defymed SAS, Strasbourg, France

²Laboratory of Experimental Surgery, Université Catholique de Louvain, Brussels, Belgium

³Ecole de Chirurgie de Nancy-Lorraine, Vandoeuvre-lès-Nancy, France

Corresponding author:

Séverine Sigrist, Defymed SAS, 8 Avenue Dante, Strasbourg 67200, France.

Email: s.sigrist@defymed.com



Creative Commons Non Commercial CC BY-NC: This article is distributed under the terms of the Creative Commons

Attribution-NonCommercial 4.0 License (<https://creativecommons.org/licenses/by-nc/4.0/>) which permits non-commercial use, reproduction and distribution of the work without further permission provided the original work is attributed as specified on the SAGE and Open Access pages (<https://us.sagepub.com/en-us/nam/open-access-at-sage>).

known as cell encapsulation, would allow transplantation of alternative cell sources, without using immune suppressive drugs. To date, efficacy of cell encapsulation has been extensively demonstrated in allogeneic conditions where physical barrier is sufficient to prevent contact between T cell and foreign cells.¹⁸ In xenogeneic situation, cell–cell contacts are not essential^{19,20} and proof of concept are scarcer. Apart from cell sources used, a bioartificial pancreas has to satisfy essential prerequisites: long-term biocompatibility, optimal conditions for survival and function of encapsulated cells, and mechanical strength to provide sustained immune protection.²¹ Devices should also be refillable and retrievable to renew cells once they are no longer functional or explant the whole system if some issues occur.²²

The first type of bioartificial pancreas was tested in the early 1980s and consisted of alginate-poly-L-Lysine microcapsules containing one or a few islets.²³ Being small in size, they allowed good oxygen exchanges²⁴ which resulted in a good viability and function of the encapsulated cells.^{25–29} This technology even reached clinical trials stage with use of both allogeneic islets in Barium-alginate microcapsules and xenogeneic islets in alginate-poly-L-ornithine-alginate microcapsules developed by Living Cell Technologies.^{30,31} However, the microcapsules are not refillable and challenging to retrieve, raising major safety and regulatory issues.²¹

The second approach involves macro-devices encapsulating a high number of cells using hydrogels or polymer membranes. Several teams developed their system and proposed the most advanced device to reach clinical phase. The first to mention is the Monolayer Cellular Device designed by Gianello and colleagues, which consists on primary islets seeded on Human acellular collagen matrix encapsulated in alginate slab. This device showed a function of encapsulated porcine islets, up to 6 months, in diabetic primates.³² The Israeli company Beta-O2 also developed their own encapsulation system, the β -Air[®] device, based on islets in alginate slab, housed in a polymer device with 0.45 μm pore membranes. The main feature of this system is a central oxygen compartment that prevents cell hypoxia but requires daily refilling using subcutaneous port. Safety and efficacy has been thoroughly demonstrated in rodents³³ and pigs³⁴ before reaching clinical trials with Human islets that essentially demonstrated safety of the system.³⁵ Viacyte was the first company to both develop a macro-device and stem cells–derived insulin-secreting cells. Their system, named Encaptra[®], consists on a pouch made of polytetrafluoroethylene (PTFE) membranes with 0.45 μm pores featuring a unique catheter for extemporaneous filling.³⁶ This device also reached clinical phase where survival of encapsulated cells occurred in few patients, while hypoxia was pointed out as the reason of cell death for other subjects.³⁷ These data highlight the main

limitation of macro-devices: a too low oxygenation level³⁸ that significantly impacts the function and viability of the cells.³⁹ Furthermore, to conciliate sufficient insulin secretion and limited size to allow safe surgical implantation, high seeding densities are used. This results in a decrease of islet viability and function⁴⁰ and potentiates effect of hypoxia.⁴¹ Finally, most of the devices currently developed cannot be refilled with new cells, and therefore require a surgical procedure to replace the whole device once cell function declines.

To overcome the limitations of current encapsulation strategies, extensive work on new membranes was initiated to select biocompatible material with high permeability for insulin, glucose, oxygen, and nutrients, associated with efficient rejection of IgG.^{42,43} These studies served as a basis to design a new bioartificial pancreas, named MailPan[®] which consists of a circular flat pouch made of semi-permeable membranes. Its key feature is an entry/exit system composed of two catheters connected to subcutaneous injection ports. Therefore, unlike most of the pre-existing encapsulation devices, MailPan[®] is first implanted empty to allow healing and vascularization of surrounding tissues, which are meant to limit cell hypoxia at the time of injection. Furthermore, entry/exit system has the advantage to allow easy replacement of cells without retrieving the whole device, extending its lifespan and avoiding repeated surgery.

This study aimed to demonstrate the safety of MailPan[®] device as well as its efficacy to provide immune protection and maintain cell function to treat type 1 diabetes (T1D). We first characterized the selectivity and pore size distribution of the membranes *in vitro* and evaluated the integration of the whole device in rat, a model allowing easy implantation of the device. Then, another *in vivo* study was performed to challenge immune protective properties of MailPan[®] in an allogeneic rat model with Major Histocompatibility Complex (MHC) incompatibility, which constitutes a relevant model with antibody response close to human physiology. Finally, the function of the device filled with a β cell line was assessed in streptozotocin-induced diabetic rats, a well characterized model in diabetes cell therapy.

Materials and methods

Chemicals

Glucose and Phosphate-buffered saline (PBS) were purchased from Thermo Fisher Scientific (Waltham, MA, USA). Fluorescein IsoThioCyanate (FITC)-IgG, FITC-Dextran, BSA, Tween 20, 4% Buffered Formol, Fetal Bovine Serum (FBS), and Sodium azide (NaN_3) were purchased from Sigma Aldrich (St. Louis, MO, USA). Streptozotocin was purchased from Santa Cruz Biotechnologies (Dallas, TX, USA).

Membrane characterization

Membranes used to manufacture MailPan[®] device are composed of biaxially oriented coextruded films made of polyester. Nanometric pores were made in films by track-etching technique consisting in beaming of films with heavy ions then opening pores using chemical components such as potassium chloride.⁴⁴ Membrane thickness was below 200 µm and surface pore diameter was smaller than 100 nm. Permeability to glucose, insulin, FITC-IgG, and FITC-Dextran was assessed in vitro, using vertical diffusion chambers, with two compartments with the same volume, separated by the membrane (membrane surface: 380 mm²). At T=0, the lower compartment of the chamber is filled with buffer and covered with the membrane, while upper compartment is filled with a solution containing 4 g/L glucose, 10 U/mL insulin (Humulin[®] R U-100, Lilly, Indianapolis, IN, USA), 13 µg/mL FITC-IgG or FITC-Dextrans (4, 20, 40, 70, 150 kDa) (n=6 samples from different membrane sheets per molecule). Buffer used is either PBS with 0.1% of BSA and 0.05% of Tween 20 for fluorescent molecules and saline solution for the others. The chamber was then incubated 24 h at 37°C. Subsequently, samples were taken from both compartments to assess the concentration of glucose using Glucose LQ[®] reagent (Spinreact, Girona, Spain), insulin by Bicinchoninic Acid (BCA) method (Quantipro BCA Assay Kit, Sigma Aldrich), and FITC-coupled molecules by fluorescence measurement (Excitation=475 nm, Emission=500–550 nm) using a plate reader. Since volume of upper and lower compartments is the same, permeability (in %) was then calculated as the ratio of the molecule concentration in the lower compartment to the sum of concentrations measured in upper and lower compartments. The maximal permeability was reached when the same quantity of molecule was detected in upper and lower compartment corresponding to a 50% value. A molecule was considered to be rejected by the membrane if the permeability was lower than 5%. This protocol is used routinely to perform quality controls on membrane batches and successfully passed method validation feasibility according to World Health Organization guide on good manufacturing practice (section 15).

The pore size was estimated by liquid–liquid porometry⁴⁵ using non-miscible liquids: isobutanol and water. Membrane disks of 47 mm diameter (n=5 from five different membrane sheets) were placed in the measuring chamber and soaked in isobutanol for 1 h at 3 mbar to completely fill the pores. Subsequently, isobutanol was flushed out of the pores using a water flux with increasing pressure injection from 0 to 8 bar. Isobutanol is flushed out from larger pores at a lower pressure compared to small pores. Quantity of isobutanol flushed out from the pores was measured, and pore size was then estimated by correlating quantity of isobutanol flushed out and water

flux pressure. Thus, high quantity of isobutanol flushed out at high pressure would reveal small pore diameter. These tests were subcontracted to Institut Européen des Membranes (Montpellier, France).

Animals

All in vivo experiments were reviewed by a local ethical committee (CREMEAS, Strasbourg, France, and CELMEA, Nancy, France) and approved by the French ministry of research, according to European Union directive 2010/63/EU. Rats were housed with unrestricted access to food and water, under controlled temperature and hygrometry following the regulatory requirements. Light dark cycle was inverted (dark period from 9:00 am to 9:00 pm) and all experiments were performed in the beginning of dark period. Function and safety studies were performed on male Wistar rats (Strain: Crl: WI (Han), Charles River Labs, Wilmington, MA, USA) aged 5 weeks at reception (body weight: 125–150 g). Experiments for bio-integration and functional imaging were conducted on male Wistar rats (Strain: RjHan: WI) acquired from Janvier Labs (Le Genest-Saint-Isle, France). For immunization study, two inbred strains of rats were used: male Lewis rats and male Dark Agouti (DA) rats both acquired from Janvier Labs, aged of 7 and 8 weeks, respectively, at the beginning of the study. All the procedures were approved under the following numbers 201508141434144 v1 (function and safety), 2016011516236430 v1 (imaging), and 2016010815212983 v2 (immunization). All in vivo protocols are summed up in Table 1.

MailPan[®] implantation

According to the patent WO2012010767, MailPan[®] device consists of a planar pouch formed with two circular polyester membranes, heat-sealed on their periphery. Two silicone catheters and titanium subcutaneous injection ports allow its filling and refilling after implantation. Device used for rat experiments displayed an external diameter 39 mm for an inner volume of 0.8 mL.

Before implantation of the MailPan[®] device, the rats were anesthetized with isoflurane to allow a tight control of anesthesia and rapid recovery. The incision area was shaved, disinfected with povidone-iodine, and a vertical incision was then performed on the side of the animal in the skin and abdominal muscles. MailPan[®] was inserted into the peritoneal cavity and stitched to the peritoneum and abdominal muscles using 4-0 suture threads passed in two rivets at the periphery of the device. Subsequently, the abdominal muscles were sutured; catheters were connected to injection ports and placed under the skin, which was then sutured. Rats were allowed to wake up on heating pads and placed in individual cages during 1 week for recovery. Post-operation care consisted in daily

Table 1. Summary of the different studies conducted in diabetic and non-diabetic rats.

Study	Model	Procedure performed	Follow up
Bio-integration	Non-diabetic Wistar rats Diabetic Wistar rats	Intraperitoneal MailPan [®] implantation Intraperitoneal MailPan [®] implantation	<ul style="list-style-type: none"> • Angiography at 2 months • PET-Scan with 4000 islets in device at 3 months • Microvessels live imaging at 6 months post-implantation (all performed on the same rats) • Plasma α2-Macroglobulin at 0, 2, 4, 6 weeks post-implantation • O₂ measurement at 6 weeks post-implantation • Histological analyses at the end of function study (4 months of implantation)
Function study	Diabetic rats	Intraperitoneal MailPan [®] implantation, pre-implantation of 6 weeks, then injection of 5.10 ⁶ RIN-m5f cells/100 g	<ul style="list-style-type: none"> • Body weight gain • Fasting and non-fasting glycemia • Viability of cells flushed out examined after 10 weeks
Immunization Study	Non-diabetic Lewis rats	Intraperitoneal MailPan [®] implantation, pre-implantation of 6 weeks, then injection of 5000 IEQ from Dark Agouti rats in device	<ul style="list-style-type: none"> • Plasma α2-Macroglobulin levels before and after cells injection • Detection of anti-Dark Agouti Antibodies at D0 and D30 after islets injection in MailPan[®]

PET: positron emission tomography; IEQ: islet-equivalent.

subcutaneous injection of Meloxicam (Metacam[®]; Boehringer, Ingelheim, Germany) at 2.5 mg/kg, until complete healing.

Cell culture and rat islets isolation

RIN-m5F (CRL-11605) cells used for function study are insulin-secreting cells derived from rat insulinoma. This cell line displays lower insulin content compared to native rat beta cells, continuously secretes insulin even at low glucose levels, and is not responsive to changes in glucose concentration.⁴⁶ These cells were purchased from ATCC (Manassas, VA, USA) and cultured on 75 cm² flasks in RPMI 1640 (Sigma Aldrich) medium supplemented with 10% FBS and 1% 100× Antibiotic-Antimycotic (Gibco[®], Thermo Fisher Scientific). One passage was realized per week by detaching cells with Trypsin-EDTA (Sigma Aldrich) and seeded at 5 million of cell in a new 75 cm² flask. Cells were transplanted at passage 33 and were negative for mycoplasma contamination.

Pancreatic islets were isolated from male Wistar rats and injected in MailPan[®] implanted on the same rat strain for positron emission tomography (PET)-Scan imaging. For immunization studies, islets were isolated from DA rats and injected in MailPan[®] implanted on Lewis rats. Animals with a body weight between 200 and 250 g were anesthetized with intraperitoneal injection of Ketamine (Imalgene[®]1000, Merial, Lyon, France) and Xylazine (Rompun[®] 2%, Bayer, Leverkusen, Germany) at a rate of 100 μ L/100 g of body weight. Islets were isolated following technique of Sutton et al.⁴⁷ based on injection of collagenase in bile duct and purification on discontinuous polysucrose gradient.

Oxygen measurement and in vivo imaging

To verify that pre-implantation enables to reach physiological oxygenation, oxygen level in MailPan[®] was measured using optic fiber oximeter (Microx Trace 4, PreSens, Regensburg, Germany) with a microsensor. Measurements were performed in devices implanted for 6 weeks in peritoneal cavity of Wistar rats (n=14, 1 measure per rat) by insertion of a 20G needle in one subcutaneous injection port of the device, to enable insertion of the microsensor.

To further investigate integration of the MailPan[®] device in intraperitoneal cavity of Wistar rats, three different imaging techniques were used successively on the same animals.

First, to visualize exchanges between the MailPan[®] and the surrounding vessels, diffusion of molecules from the device to blood circulation was assessed by angiography using X-ray and a signal amplifier (Arcadis, Siemens). Two months after device implantation, anesthetized Wistar rats (n=3) received iodixanol (Visipaque[®] 320, molecular weight: 1.55 kDa, GE Healthcare, Chicago, IL, USA) into the MailPan[®] implanted in the peritoneal cavity. Repeated acquisitions were made during up to 150 min to observe the decrease in signal intensity, demonstrating the diffusion of the contrast product out of the device.

One month later (i.e. 3 months after implantation), PET-Scan was used to assess whether glucose enters into the device implanted in the rat. To be able to visualize glucose flux entry, 4000 islet-equivalent (IEQ) were injected into the device implanted in the peritoneal cavity of Wistar rats (n=3). Five days after islets injection, rats were fasted for 12h and received two oral administrations of Acipimox (Olbetam[®], Pfizer, New York, NY, USA) to enhance glucose absorption, before IV injection of 18-fluorodeoxyglucose

(18-FDG) (Flucis[®], Cisbio, Codolet, France). Acipimox inhibits peripheral lipolysis, reduces plasma free fatty acid levels, and stimulates myocardial glucose utilization. This creates a driving force resulting in an enhanced distribution of 18-FDG in blood circulation to reach all organs of interest. Signal acquisition was done using Inveon[®] (Siemens, Munich, Germany), a device adapted to small animals. The rats were anesthetized for the procedure and placed on heating pads during the whole duration of the experiments.

Finally, microvessels around MailPan[®] were visualized using orthogonal polarized spectral imaging (Microscan[®], MicroVision Medical, Amsterdam, Netherlands) at 6 months post-implantation in peritoneal cavity of Wistar rats (n=4). Under isoflurane anesthesia, a 2 cm incision was performed to access the device with surrounding tissues and to insert the Microscan[®]. Analysis software allowed performing quantifications on the acquired fields for each animal, to measure vessel length, surface, density, and determine if they are perfused. Diameter of vessels was also measured to determine the most frequent size range observed.

Histological analysis

At the end of function study, MailPan[®] devices were retrieved (n=6) after a total implantation time of 4 months (decomposed as 6 weeks of pre-implantation, 8 weeks of follow-up, and 2 weeks after cells retrieving), and surrounding tissues fixed in 4% buffered formol. Histological analyses were performed by an independent pathologist (Laboratoire des Contades, Strasbourg, France), based on Masson's trichrome staining to visualize vascularization and appreciate inflammatory status of surrounding tissues.

Function study

Diabetes was induced in male Wistar rats by a unique intraperitoneal injection of 75 mg/kg of streptozotocin. Diabetic rats displayed non-fasting glycemia higher than 5 g/L, then non-fasting plasmatic C-peptide levels were measured by ELISA (Rat C-peptide ELISA kit, Mercodia, Uppsala, Sweden) 6 days after the streptozotocin injection, and the rats with concentration below 150 pmol/L were selected for further steps of the study. Age matched litter mate Wistar rats did not receive streptozotocin injection and were kept as non-diabetic controls (n=3).

Selected animals received subcutaneous insulin implants (Linplant[®], Linshin, Toronto, Canada) with a daily dose of 3 IU and randomized in either MailPan[®] group to receive cells (n=6) or diabetic control group (n=4).

After 6 weeks following MailPan[®] implantation, 5 million of single RIN-m5F per 100 g of body weight were injected in device using subcutaneous ports. For injection,

cells were detached using Trypsin-EDTA then washed in RPMI-1640 with 1% of penicillin/streptomycin. Before inserting needles, the skin of the animal was shaved and disinfected. Cells were injected in 300 μ L of RPMI-1640 with 1% of penicillin/streptomycin. A metabolic follow-up was set up to assess the function of the MailPan[®] with RIN-m5F cells. The body weight was measured weekly, and fasting capillary glycemia was recorded using a glucometer. In one rat with RIN-m5F cells inside the MailPan[®], Oral Glucose Tolerance Test (OGTT) (2g/kg of glucose) were performed before and after cell flushed out at 10 weeks. Viability of retrieved cells was analyzed on a fluorescence microscope (Eclipse 50i, Nikon, Amstelveen, Netherlands) using simultaneous staining with Calcein AM (for live cells) and Ethidium homodimer-1 (for dead cells) (Live/Dead Viability/cytotoxicity kit, Invitrogen, Carlsbad, CA, USA). Viability of cells retrieved from MailPan[®] was quantified for each recipient on at least 10 clusters, as a ratio of fluorescence intensity measured with Calcein AM staining on the sum of fluorescence intensities measured with both Calcein AM and Ethidium homodimer-1. Analyses were performed using Nis-Element-BR software (Nikon, Amstelveen, Netherlands).

Immunization study

Lewis rats (MHC: RT1^l) were used as recipients and DA (MHC: RT1^{av1}) rats as islet donors, to have MHC mismatch. Lewis rats (n=6) were first implanted with MailPan[®] device 6 weeks before injection of islets to allow healing and neovascularization of tissues surrounding the device. Pancreatic islets were then isolated from DA rats (8 DA rat used per recipient) and injected into the MailPan[®] of Lewis; 5000 IEQ (dose ~15,000 IEQ/kg) were injected per recipient in 300 μ L of CMRL-1066 (Gibco[®], Thermo Fisher Scientific) with 1% penicillin/streptomycin. In parallel, equal quantity of islets was injected subcutaneously to Lewis rats without MailPan[®], as positive controls.

The first series of blood samples was taken in heparinized tubes from the Lewis rats with MailPan[®] before device implantation, at 1, 2, and 4 weeks after device implantation, and at 0, 1, 2, 4 weeks after islets injection. Plasma was collected to determine the α 2-Macroglobulin (α 2M) plasma levels using ELISA assay (Rat α 2-Macroglobulin ELISA Kit, Abcam, Cambridge, UK) following manufacturer's instructions.

The second series of blood samples was collected from the Lewis rats with MailPan[®] as well as from the controls, at 0 and 4 weeks after DA islets injection. The obtained serum was used to detect antibodies against DA islets in order to assess whether the MailPan[®] can prevent immunization of the recipients against transplanted cells. Briefly, freshly drawn, whole heparinized blood was diluted with Hanks' Balanced Salt Solution (HBSS), and the peripheral blood mononucleated cells (PBMCs) were obtained by

gradient centrifugation (Ficoll-Paque[®] Plus, GE Healthcare) and washed with HBSS. Approximately, 250,000 freshly isolated PBMCs were incubated with Lewis recipients decomplemented sera for 30 min at room temperature, followed by washing using HBSS with 0.5% FBS and 0.1% sodium azide. Subsequently, 5 µg/mL of goat anti-rat IgG secondary antibody Alexa Fluor 488 (Thermo Fisher Scientific) was added and incubated for 30 min at room temperature, before washing. Cells were analyzed with BD FACSCalibur and CellQuest Pro software (BD Bioscience, Franklin Lakes, NJ, USA). A positive reaction was defined as a shift of more than 10-channels in mean fluorescence intensity (MFI) of donor lymphocytes with post-transplantation (Day 30) serum as compared to the MFI with pre-transplant serum (Day 0).

At the end of the study, the tightness of MailPan[®] explanted from each recipient was carefully investigated. To avoid bias, this investigation was performed before collecting results of anti-DA antibodies detection in the serum of recipients.

Data analysis

Graphs and statistical analyses were performed with Prism V 7.04 (GraphPad Software, San Diego, CA, USA). Results are shown as mean ± SEM. After verifying the normality of value distribution using Shapiro–Wilk test, one-way analysis of variance (ANOVA) was used for α2M levels, weight, and non-fasting glycemia area under the curve (AUC) values. Two-way ANOVA was used for fasting and non-fasting glycemia follow-up. For all analyses, a Tukey post hoc test for multiple comparisons was performed. Difference between two conditions was considered as statistically significant at $p < 0.05$.

Results

Device design and permeability

MailPan[®] device consists of a circular planar pouch made up of thermoplastic membranes connected to two catheters with injection ports that are used to inject cells and to replace them when necessary (Figure 1(a)). These features allow implantation of the whole device without cells (Figure 1(b)) to allow pre-vascularization (Figure 1(c)). This provides an optimal environment for the cells injected after a post-implantation period (Figure 1(d)).

The function and safety of a bioartificial pancreas is dependent on the selectivity of the membranes. We have assessed the selectivity in vitro in static conditions, by estimating the membrane permeability to glucose, insulin, and Human IgG. After 24 h of incubation, both glucose and insulin diffused through the membrane and approached the maximal permeability value of 50% ($45.93 \pm 1.25\%$ and $38.11 \pm 1.18\%$, $n=6$ for glucose and insulin, respectively). In the same experimental conditions, we observed a very

low permeability of the membrane to Human IgG ($1.77 \pm 0.33\%$, $n=6$), indicating efficient rejection of this molecule (Figure 2(a)). The permeability of the membranes to different sizes of Dextran was then assessed to determine their molecular weight cut-off. Dextran with size ~4 kDa efficiently crossed the membranes, with a permeability of ~30%. As expected, an increase in Dextran size resulted in an important decrease of permeability for molecules with a size of 20 and 40 kDa. Testing of Dextran with a size of 70 kDa resulted in a permeability lower than the rejection threshold ($1.47 \pm 0.20\%$, $n=6$). The results helped to estimate the rejection cut-off around 55 kDa (Figure 2(b)).

Pore size distribution across the membrane was assessed using liquid–liquid porometry on five different samples. Results showed a mean pore diameter of 11–16 nm, with extreme values of 8–72 nm (Figure 2(c)). Pore size distribution (Figure 2(d)) revealed a narrow distribution around the mean value, indicating a homogeneous pore size distribution.

Bio-integration and functional imaging

Bio-integration of MailPan[®] was assessed in the peritoneal cavity of diabetic rats. Recovery of the animals was fast and no adverse effects were observed on both non-diabetic and diabetic rats. Passage of the catheters used to fill and empty the device, from the intraperitoneal to the subcutaneous, did not cause any healing or contamination issues. Skin disinfection protocol performed prior to insert needles into subcutaneous ports was efficient to prevent bacterial contamination of the implanted devices.

To assess acceptance of the whole device in intraperitoneal in rat, plasma levels of α2M, a global inflammatory marker were assessed upon MailPan[®] implantation. Mean plasma levels showed a significant increase ($p < 0.001$) at 2 weeks post-implantation and decreased in subsequent weeks, with concentrations similar to those observed at $T=0$ after 6 weeks. These results demonstrated the absence of chronic inflammation and helped to determine an optimal pre-implantation period of 6 weeks before cells injection, to ensure total resorption of post-surgical inflammation (Figure 3(a)). To confirm that this pre-implantation period is also sufficient to limit hypoxia and support cell survival and function, oxygen concentration was then measured inside the device at 6 weeks post-implantation. Results showed heterogeneity in the values measured, with a 95% confidence interval of median ranging from 4.4% to 12.2% (equivalent to 32.66–90.55 mmHg, $n=14$). However, most of the values were higher than 5% (37.1 mmHg), showing the absence of severe hypoxia inside the implanted device (Figure 3(b)). As a comparison, same measurements performed less than 1 week after MailPan[®] implantation revealed low oxygen levels, smaller than 1% (7.42 mmHg). Retrieval of the device from the peritoneal cavity of diabetic

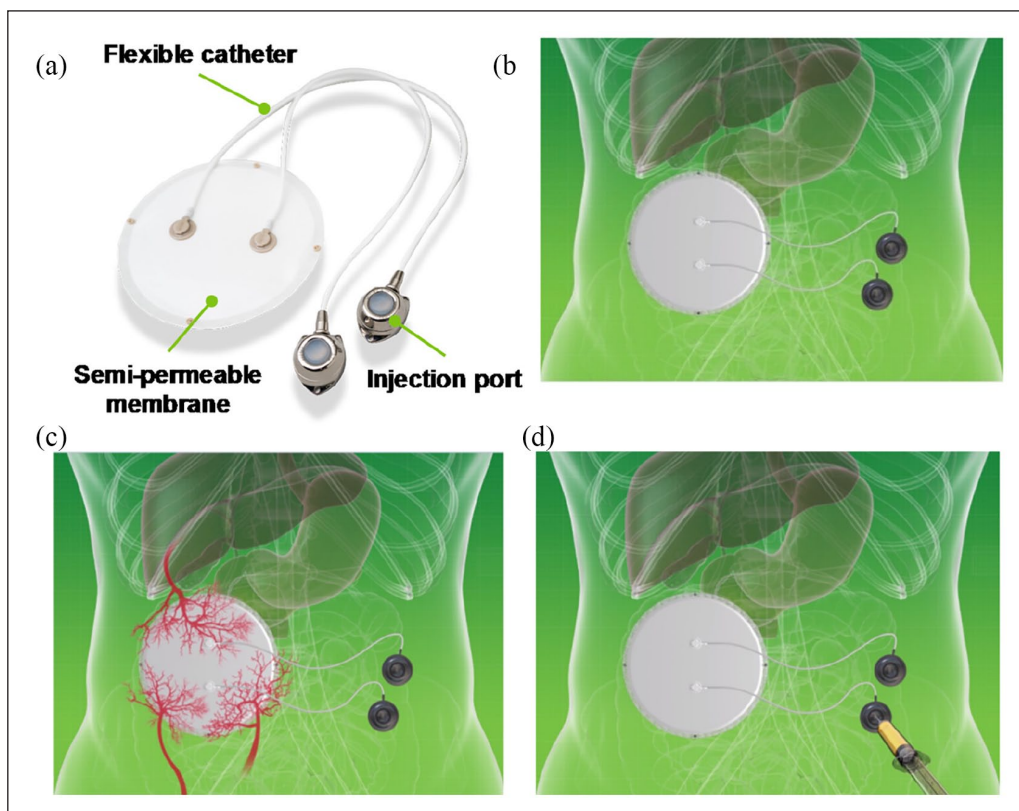


Figure 1. Principle of MailPan® device: (a) The device consists of a planar pouch with two catheters with injection ports, (b) it is first implanted without cells, (c) to allow healing and neovascularization around the device, and (d) once healing and neovascularization period of 6 weeks was completed, insulin-secreting cells were injected via subcutaneous ports.

rats after 4 months of implantation revealed an excellent integration at the implantation site. Only a few adipose pads were observed at the periphery of the device (Figure 3(c)), and a thin tissue layer with macroscopically visible blood vessels was found in direct contact with the membranes (Figure 3(d)). Consistently, histological analyses performed on this thin tissue found on membranes showed low fibrosis (~0.1 mm thick) and high density of vessels (Figure 3(e)). Complementary analyses were performed on vascularization of tissues surrounding the MailPan® after 6 months of implantation using orthogonal polarized spectral imaging that allows direct imaging of small vessels. Results showed a dense vascularization around the device, with heterogeneous vessel size from 25 to few micrometers, revealing presence of an organized vascular network (Figure 3(f)). Furthermore, measure of vessels diameter indicated that a large majority of the vessels in the tissues surrounding the device are smaller than 15 μm (Figure 3(g)), reflecting a well-organized and functional vascular network. Imaging technique also enabled to directly observe the blood flow around the device (Movie S1). Quantifications performed revealed that all vessels observed were perfused, with $15.10 \pm 3.86\%$ of the field of view occupied by vessels, indicating a high vascular density and efficient perfusion of tissues around the device (Table 2).

PET-Scan imaging was performed to assess quality of exchanges between the device and its surrounding vascularization; 18-FDG showed normal distribution pattern, with high signal intensity in heart, accumulation in bladder, and elimination via the urinary tract. In parallel, a mid-intensity signal was observed in a circular area corresponding to the place of MailPan® device filled with 4000 rat islets. This constitutes a direct proof of the efficient diffusion of the glucose into the pouch (Figure 4(a)). Another group of rats with MailPan® were treated with iodinated contrast product in the device to perform angiography. Results highlighted a progressive decrease of the signal observed in the pouch associated with an increase of the signal in kidneys and bladder, confirming the presence of a functional vascular network around the MailPan® (Figure 4(b)). Overall, these results show a very satisfying bio-integration of the device, surrounded by a functional vascularization.

Function in diabetic rats

After demonstrating the relevance of membranes used and successful bio-integration of the whole device, its ability to normalize glycemia once filled with insulin-secreting cells was investigated.

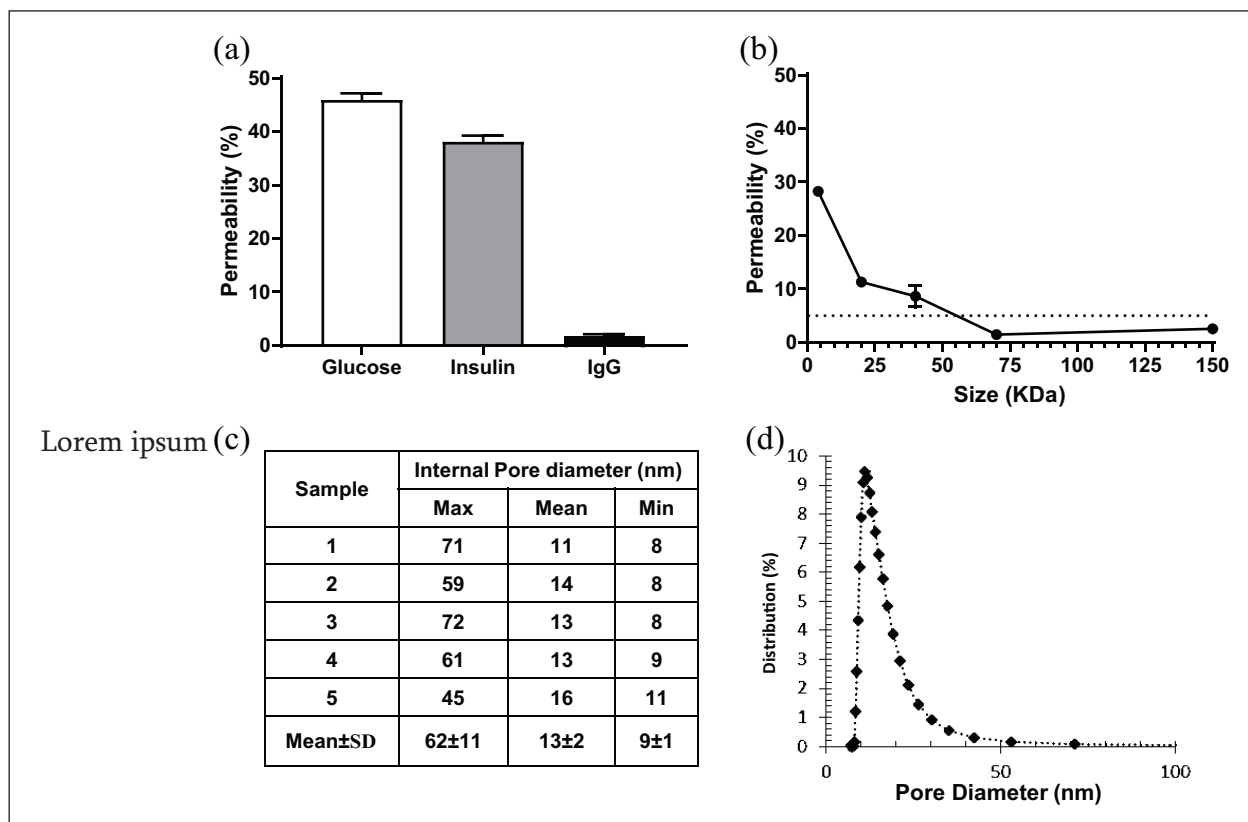


Figure 2. Permeability of membranes used for MailPan[®] is suitable for insulin-secreting cells encapsulation: (a) Permeability of membranes to glucose, insulin, and IgG assessed in static conditions after 24 h of incubation at 37°C, mean \pm SEM, $n=6$ for each molecule; (b) permeability of membrane to fluorescent dextran related to molecular weight, in static conditions after 24 h of incubation at 37°C. The horizontal dotted line represents the cut-off threshold set at 5% of permeability, mean \pm SEM, $n=6$ for each Dextran size; (c) pores size measurement by liquid-liquid porometry performed on five membrane samples; and (d) representative distribution of pore size on membrane samples tested.

Six weeks after implantation of MailPan[®] in the peritoneal cavity of diabetic rats, single RIN-m5F cells were injected into the device and exogenous insulin therapy was stopped 2 weeks after. Injection of cells resulted in the maintenance of body weight gain, in the absence of insulin therapy, comparable to non-diabetic control rats. Conversely, diabetic control animals showed a rapid weight loss immediately after the removal of insulin implants at D14 ($102.7 \pm 5.9\%$ at D14 vs $85.1 \pm 6.3\%$ at D24, $n=4$ each time) (Figure 5(a)). It resulted in significantly higher AUC of weight gain curves for diabetic rats with MailPan[®] filled with RIN-m5F compared to diabetic controls ($p < 0.005$) (Figure 5(b)). Filling of the device with cells also normalized fasting glycemia, to reach values comparable to non-diabetic rats and significantly lower ($p < 0.001$) than diabetic control at each timepoint tested (Figure 5(c)).

However, non-fasting glycemia was only partially corrected with mean values ~ 4 g/L in RIN-m5F group versus 6 g/L for diabetic controls (Supplemental Appendix, SI-1).

Cells flush out from implanted MailPan[®] device was performed in one animal, with OGTT performed before and after the procedure. Results clearly showed a

normal response to glucose stimulation when cells were in the device, which was impaired after flushing out the cells (Supplemental Appendix, SI-2 A). These results confirmed that the observed function was specific to encapsulated cells. A trend to obtain near-hypoglycemia values was observed in the beginning and at the end of the follow-up. This can be directly related to the C-peptide level, which was notably high, when cells were in the device. A dramatical decrease was then observed after flushing out the cells (Supplemental Appendix, SI-2 B).

Live/dead staining of the cells flushed out from the device after 10 weeks showed that single cells formed clusters with mean viability higher than 65% for all recipient (minimum, recipient 2: 66.13%; maximum, recipient 4: 84.43%) (Figure 5(d)). Morphology and size of clusters formed within the MailPan[®] was comparable to rat islets (Figure 5(e)).

Immunization study

One of the essential functions expected from a bioartificial pancreas is to protect encapsulated cells from the immune

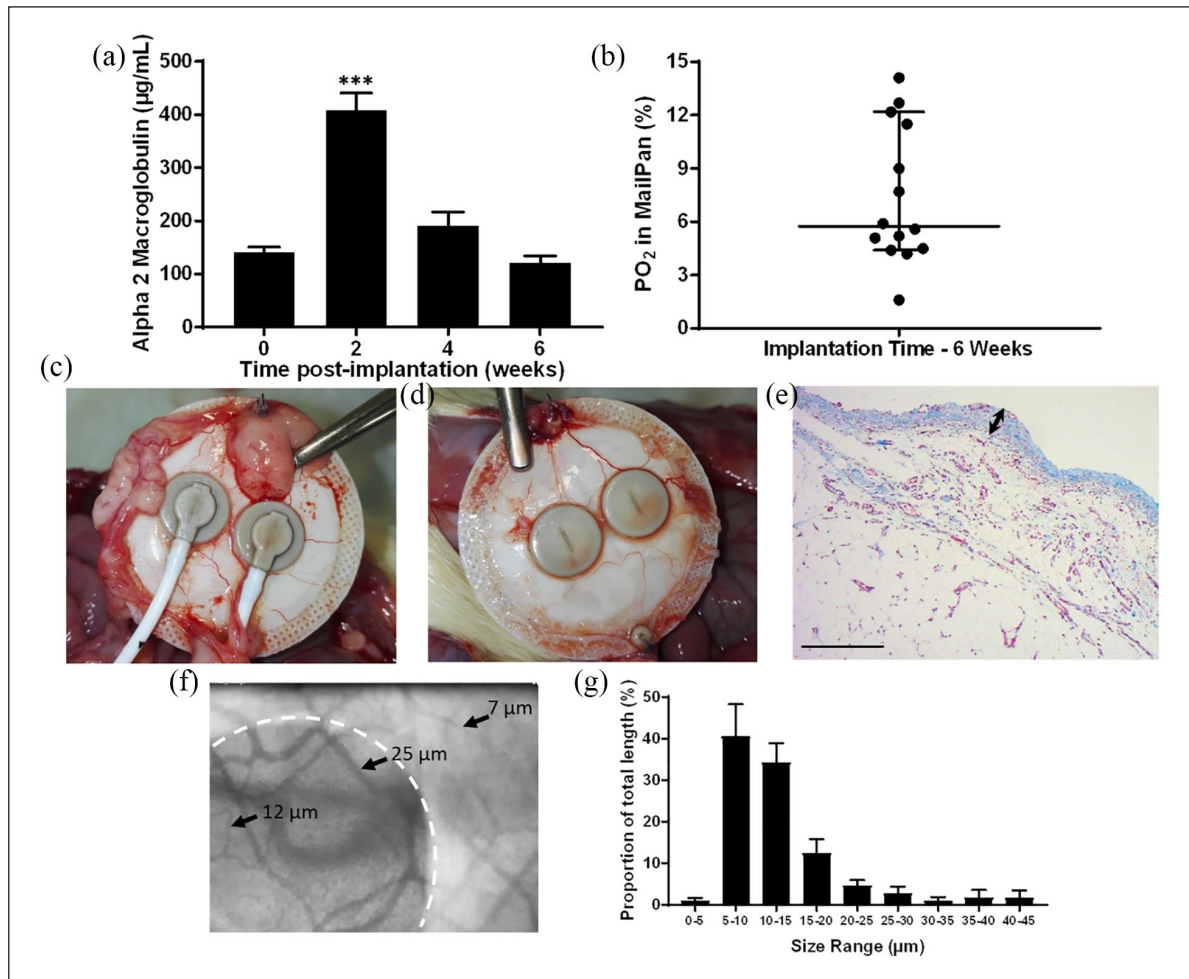


Figure 3. MailPan® device shows good tissue integration and vascularization in rats: (a) Plasma levels of α 2-Macroglobulin following implantation of empty MailPan® in the peritoneal cavity of diabetic rats ($n=6$), mean \pm SEM, *** $p < 0.0001$ vs $T=0$; (b) Oxygen concentration in the MailPan® at 6 weeks post-implantation in diabetic rats. Each point corresponds to measurement in one animal ($n=14$), horizontal bar shows median and vertical bars indicate 95% confidence interval; (c–d) retrieving of the MailPan® from the peritoneal cavity of diabetic rats after 4 months of implantation. Representative pictures of $n=6$ animals; (e) Masson's trichrome staining performed on tissues surrounding the device after 4 months of implantation in the rat. Pictures are representative of $n=6$ animals. Scale bar corresponds to 200 μ m and double arrow shows the thickness of fibrous tissues in direct contact with the device at retrieving; (f) live imaging using orthogonal polarized spectral imaging of small capillaries in tissues surrounding the MailPan® at 6 months post-implantation in non-diabetic rats, with device position highlighted with a white dotted line, and size of few vessels observed indicated with black arrows. Representative of $n=4$ animals; and (g) size distribution of vessels surrounding MailPan® after 6 months of implantation in peritoneal cavity on rats, calculated from live imaging. Results are represented for each size range as a proportion of total vessel length, with SEM as error bars ($n=4$).

Table 2. Quantitative analysis of vasculature in tissues surrounding MailPan® implanted for 6 months in peritoneal cavity on rats. Results obtained with orthogonal polarized spectral imaging on $n=4$ rats implanted with MailPan in peritoneal cavity.

Rat	Vessel length (mm)	Vessel density (mm/mm ²)	Vessel surface (%)	Perfused vessels (%)
1	2.65	5.37	6.89	100
2	5.86	9.20	10.38	100
3	10.94	16.58	19.90	100
4	8.20	13.22	23.24	100
Mean \pm SEM	6.91 \pm 3.52	11.09 \pm 4.86	15.10 \pm 7.72	100 \pm 0

system of the recipient. This was challenged by the use of Lewis as recipients and DA as donors, two inbred strains with discordant MHC.

The α 2M levels measured in plasma of the recipient after injection of DA islets in the device did not show any increase compared to pre-injection time. A decrease

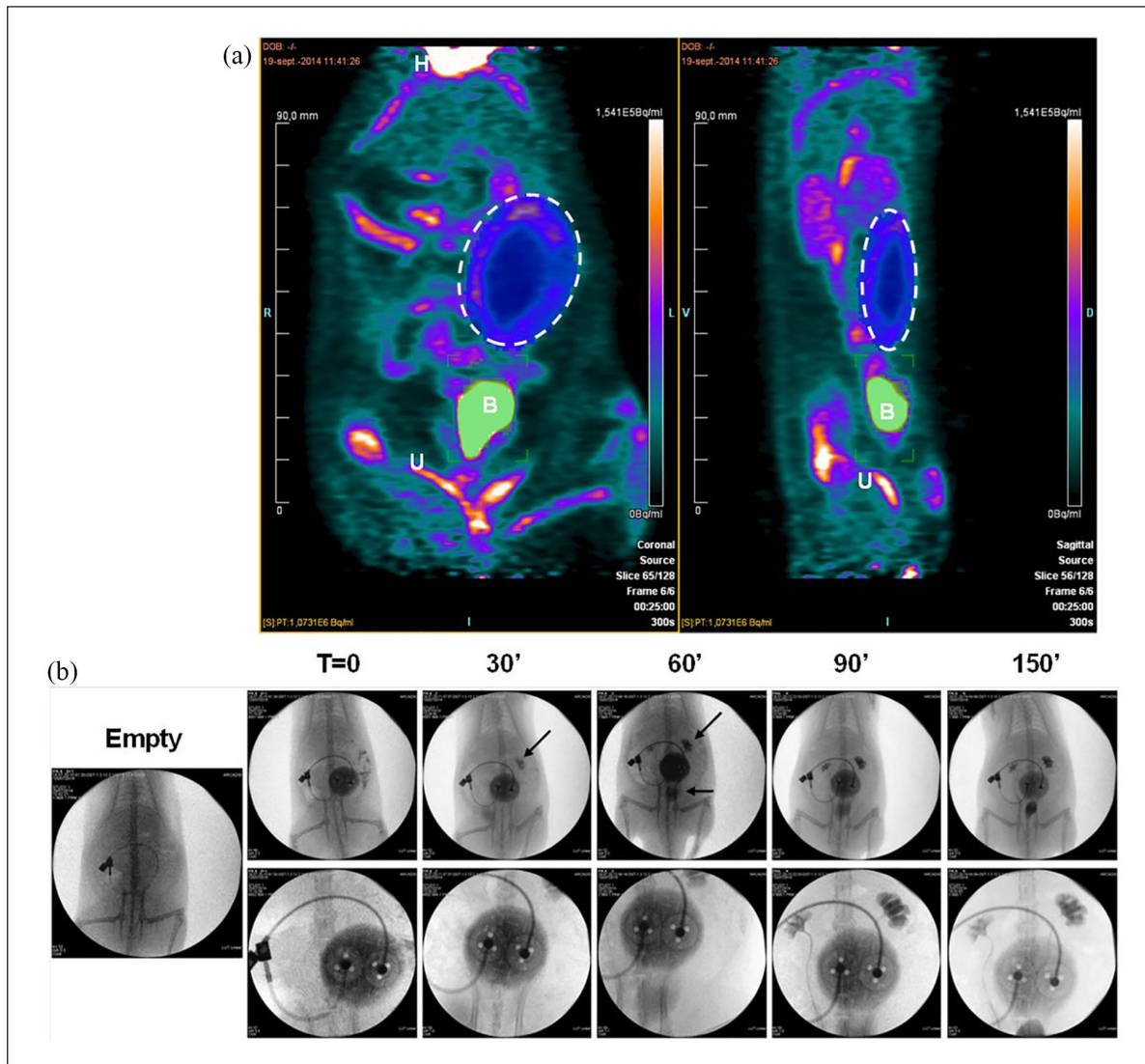


Figure 4. Pre-vascularization of the device allows efficient exchanges with blood circulation: (a) PET-scan performed 2 days after injection of 4000 rat islets in the MailPan[®] after 3 months post-implantation in the peritoneal cavity of non-diabetic rats. Picture shows signal accumulation in the area of MailPan[®] device indicating the entry of glucose. Representative pictures of $n=3$ experiments, dotted circle highlight MailPan[®]'s position. H: heart, B: bladder, U: urinary tract and (b) injection of angiography contrast product in MailPan[®] in the peritoneal cavity of rats with a 150 min follow-up. Arrows highlight the accumulation of contrast product in kidney starting 30 min and in kidney and bladder starting 60 min. Upper panel show view of the whole abdomen and lower panel a close-up of MailPan[®] device. Representative pictures of $n=3$ experiments.

is even observed at 2 and 4 weeks post-injection ($121.1 \pm 12.9 \mu\text{g/mL}$ at $T=0$; $66.8 \pm 7.1 \mu\text{g/mL}$ at 4 weeks, $n=6$ each time, $p < 0.01$), demonstrating absence of inflammatory response triggered by cells injected in the MailPan[®] (Figure 6(a)). Immune response was then assessed by flow cytometry, by detecting, via a fluorescent secondary antibody, potential binding of antibodies from recipients' serum on PBMCs donor rat strain. Tests performed before injection showed the absence of fluorescence signal. This indicates that no antibodies from recipient serum bound

on PBMCs from DA rats, confirming the native status of the recipients (Figure 6(b), left panel). Tests were repeated at 30 days post-injection and showed an increase in fluorescent signal compared to $T=0$, after free subcutaneous injection of islets. In contrast, profiles obtained after injection of islets in the MailPan[®] were comparable to pre-transplantation state (Figure 6(b), right panel). Examination of the devices after retrieval showed the absence of damage and preserved tightness, correlating integrity of the device with immune protection.

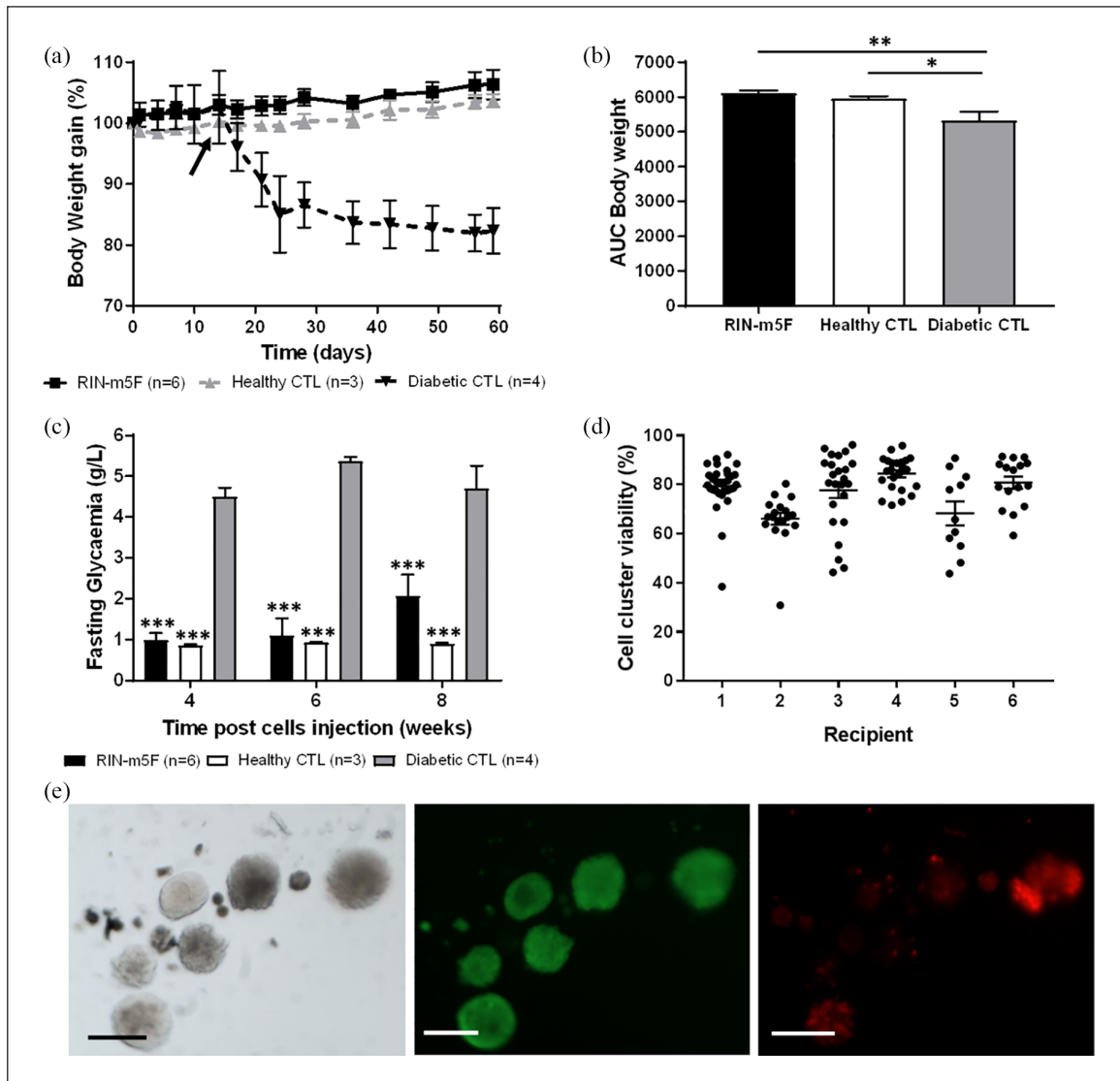


Figure 5. MailPan[®] filled with RIN-m5F cells can correct diabetes in STZ-induced rats: (a) Body weight gain follow-up; (b) AUC calculated from weight gain values of the whole follow-up of rats that received RIN-m5F cells in MailPan[®] (RIN group n = 6), healthy control (n = 3), and diabetic control (n = 4). Mean \pm SEM. * $p < 0.05$; ** $p < 0.01$ one-way ANOVA. On graph A, black arrow indicates the time (D14) when exogenous insulin therapy was stopped; (c) fasting glycaemia of rats that received RIN-m5F cells in MailPan[®] (RIN group n = 6), healthy control (n = 3), and diabetic control (n = 4). Mean \pm SEM. *** $p < 0.001$ vs diabetic control, two-way ANOVA; (d) viability of cell clusters recovered from the MailPan[®] of each recipient after 10 weeks. Viability expressed in percent was calculated using live/dead staining. Each point represents a cluster analyzed; horizontal bar shows mean value with SEM as error bars; and (e) representative picture of Live/dead staining performed on cells cluster recovered after 10 weeks in the device. From left to right are presented pictures of bright field, calcein AM staining (live cells) and Ethidium Homodimer-1 staining (dead cells). Scale bar represents 200 μ m.

During the same study, one of the rats was implanted with a device damaged by a needle upon implantation procedure and filled with 5000 IEQ from DA rats. It resulted in a consequent increase of α 2M 1 week after islets injection (69.3 μ g/mL at T=0 vs 473.4 μ g/mL at 1 week). Consistently, flow cytometry profile obtained 30 days post-injection of islets in the pierced device of this rat was comparable to those obtained after free subcutaneous injection revealing immunization of the recipient (Supplemental Appendix, SI-3).

Discussion

Advances in stem cells differentiation protocols resulted in the successful generation of insulin-secreting cells, available in inexhaustible quantity^{48–50} which would enable to bypass pancreas shortage limiting cell therapy application to treat T1D.^{6–8} However, the hurdle related to the use of chronic immune suppressive treatment remains while their safety for the patient is questioned with risks of teratoma formation.^{14–16} These limitations could be addressed with

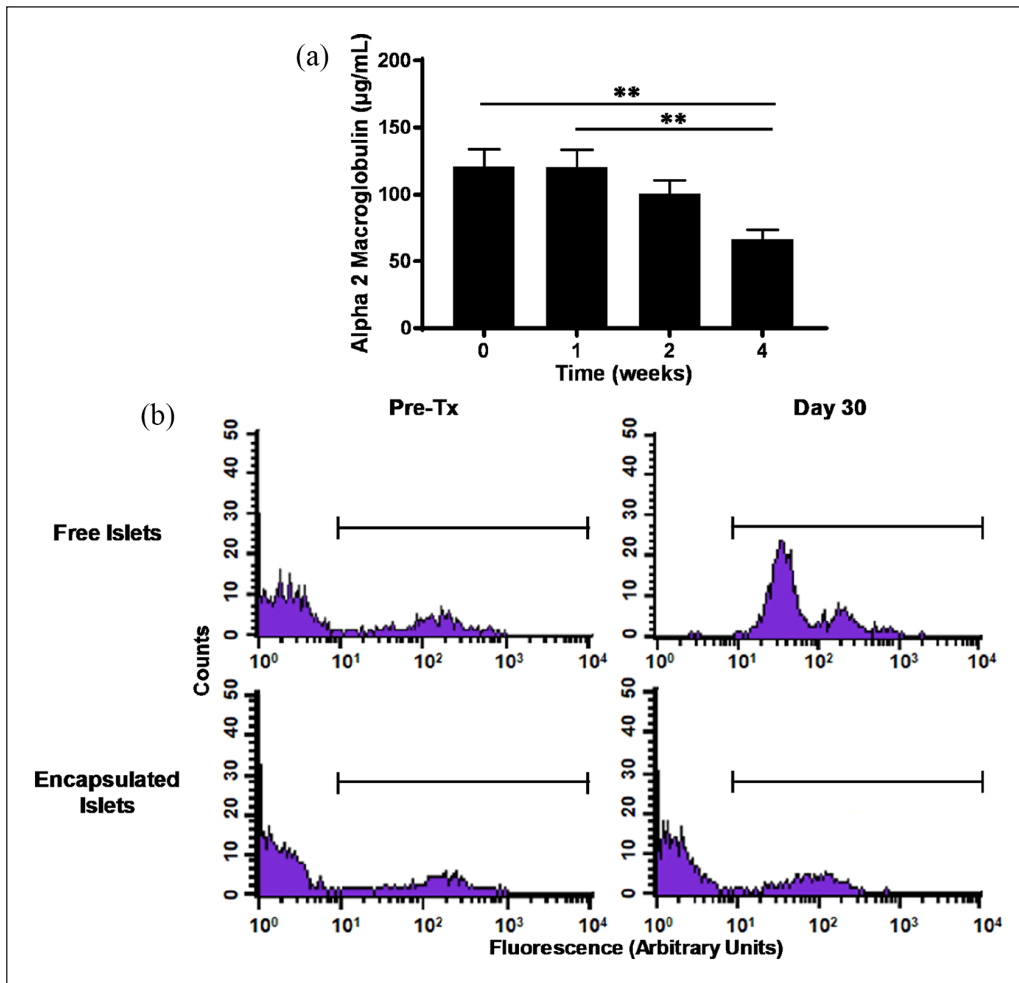


Figure 6. MailPan[®] device prevents immunization of Lewis rat recipients against allogeneic islets: (a) Plasmatic levels of α 2-Macroglobulin in recipients, after injection of 5000 allogeneic IEQ (T=0). Mean \pm SEM, n=6. ** for $p < 0.01$ and (b) presence of anti-Dark Agouti antibodies in serum of Lewis recipients assessed by flow cytometry, before and 30 days after free subcutaneous injection of 5000 IEQ from Dark Agouti (upper panel) or after their encapsulation in MailPan[®] (lower panel). Representative profile of n=6 animals. The horizontal line indicates the cell population considered as positive.

the use of a bioartificial pancreas that can protect the recipient from transplanted cells and cells from immune response, without compromising their survival and function.

In vitro testing of the membranes was based on 24-h end-point incubations with a system used and continuously refined since the early stage of MailPan[®] development.⁴² Use of this system does not allow calculation of flux or diffusion coefficient. Further experiments with commonly used systems, such as perfusion, could be performed to be able to calculate such parameters and compare with other encapsulation membranes. However, our in vitro tests revealed a mean pore diameter around 10nm, and an efficient rejection of human IgG by the membranes. This is in accordance with the membrane molecular weight cut-off of 55 kDa which is smaller than a Human IgG (~150kDa).³⁸ Another team developing a cubic encapsulation device showed in vitro a total

blockade of IgG with pores of 78 nm diameter, larger than in MailPan[®] membranes.⁵¹ This suggests that pore size is not the only parameter to consider in such tests, highlighting a potential role of material or structure interactions with the IgG. In vivo, we demonstrated that MailPan[®] device prevents formation of antibodies against encapsulated allogeneic cells in the case of incompatible MHC between donor and recipient rats. Given the high quantity of serum needed related to the animal model, we only investigated antibodies formation before and 30 days after cells injection in device. Indeed, if IgG response can be detectable after only 14 days, encapsulation can delay this response, as previously observed in case of microencapsulated pig islets transplanted in mice, where peak of IgG response was detected at 30 days post transplantation.⁵² In addition, our positive controls that received free islets, in the subcutaneous site, harbored an important IgG response after 30 days. Immune protection provided by MailPan[®]

device is consistent with the work of Colton⁵³ who estimated that a pore size below 30 nm would provide immune protection. Such immune protective properties found for MailPan[®] were only indirectly reported with other devices by comparing graft efficacy of either allogeneic versus xenogeneic islets⁵⁴ or isogeneic versus allogeneic islets³³ in diabetic rodents. However, unlike observed in allogeneic situation, xenorejection involves indirect pathway that does not require direct contacts between host immune cells and transplanted cells.¹⁹ It means that small antigens from transplanted cells, able to cross the membrane of encapsulation device, could be processed by antigen presenting cells and trigger immune response.⁵² Based on the molecular weight cut off (55 kDa) that we determined for MailPan[®] membrane, diffusion of small porcine antigens such as α -Gal epitope is probable and could induce humoral response, as reported previously with alginate-encapsulated porcine islets transplanted in primate.³² This confirms the need for additional immunization studies in xenogeneic conditions.

A bioartificial pancreas must also be safe for the recipient. As far as stem cell-derived insulin-secreting cells or xenogeneic islets could be used in encapsulation devices, their safety is closely related to the capacity to prevent the exit of the encapsulated cells. Here, pore diameter measurement, absolute integrity of retrieved devices, and absence of immunization of the recipient against allogeneic islets showed that MailPan[®] efficiently retains the cells. This constitutes an advantage of our device compared to conventional alginate microencapsulation facing recurrent cells protruding.^{55,56} Our device also showed excellent biocompatibility without chronic inflammation, as highlighted by α 2M levels. The only peak of this marker detected in our conditions was transient, related to surgical procedure and resorbed before cells filling in the MailPan[®]. Moreover, post-implantation histological analyses performed up to 6 months showed normal healing of the surrounding tissues with thin fibrous tissue confirming an excellent integration of the MailPan[®].

While protecting both the recipient and encapsulated cells, optimizing the function and survival of the later is the key point for a bioartificial pancreas. To address this problem, device design features subcutaneous entry/exit ports to allow pre-vascularization of the system before cells filling. Oxygen measurement performed at the end of the pre-vascularization period of 6 weeks in diabetic rats revealed satisfying oxygenation of the device. Most of the values were equal or higher than 5% of oxygen (37.1 mmHg), corresponding to the oxygen level measured of vascularized islets in the pancreas,⁵⁷ thus demonstrating the efficacy of pre-vascularization step. Furthermore, direct imaging of vessels revealed well-organized vascular network mainly composed of small capillaries (<15 μ m diameter), with functional vascular density that appeared to be higher than observed with other cell encapsulation devices.^{58,59} If some teams reported a

progressive decrease of oxygen levels in their device filled with islets,⁵⁸ another study surprisingly demonstrated increase in local oxygen saturation when cells were present.⁶⁰ In vitro study on the combined effect of high seeding density and hypoxia highlighted the critical impact of initial oxygen levels in medium, as it potentiates deleterious effect of high cell density.⁴¹ However, it has been shown that these effects also depend on the cell type used, with higher resistance of stem cell-derived insulin-secreting cells compared to human or mouse islets.⁶¹ Consequently, if pre-vascularization period observed after MailPan[®] implantation should help to limit the effect of high seeding density, further work has to be done to correlate quantity of cells in the device, oxygen levels, and function in diabetic rats. Moreover, apart from oxygen, survival and function of cells is also dependent on the flux of larger molecules such as glucose, through the membranes of the device. Here, PET-Scan revealed rapid entry of glucose in MailPan[®] filled with rat islets and angiography revealed quick exit of contrast product. These two findings demonstrate that vascularization surrounding the device can support dynamic exchanges with the pouch. Function study performed with MailPan[®] filled with a rat beta cell line in diabetic rats aimed to approach future clinical setting, with the use of allogeneic insulin-secreting cells rather than purified islets. Results clearly showed metabolic effects of the cells with normalization of fasting glycemia and body weight gain all over the 8 weeks of follow-up, mainly due to the capacity of RIN-m5F cells to constantly secrete insulin. However, non-fasting glycemia was not fully normalized since RIN-m5F have low responsiveness to glucose increase within physiological range.^{46,62} This was confirmed in vivo with high C-peptide levels even in fasting condition and limited increase (1.3-fold) upon glucose administration. This resulted in OGTT profile comparable to non-diabetic rats in few animals, but often led to severe hypoglycemia that obliged us to rapidly stop the follow-up. This is in accordance with data obtained in diabetic rats where implantation of slow-releasing insulin pellets was sufficient to normalize Intravenous Glucose Tolerance Test (IVGTT) profile.⁶³ We also succeeded to normalize OGTT profile with device filled with allogeneic rat islets but with variability of response related to primary culture heterogeneity (data not shown). Other teams developing their encapsulation system showed regulation of both fasting and non-fasting glycemia in diabetic rats. After subcutaneous implantation of their device filled with rat islets, Barkai et al.³³ showed non-fasting glycemia regulation in diabetic rats for up to 90 days and normalization of IVGTT. Nevertheless, it required daily oxygen infusion via subcutaneous port to maintain islet function, and no C-peptide data were presented. More recently, a polymer thread used to carry alginate-encapsulated rat or human islets gathered solid function data, normalizing glycemia and intraperitoneal glucose tolerance test (IPGTT) for up to 6 months in

diabetic rats.⁵⁴ These encouraging results were obtained with pancreatic islets and partly rely on the good function of this cell type. Though less frequent as primary islets, use of encapsulated stem cells–derived insulin-secreting cells also gave positive results. Agulnick et al.⁶⁴ showed a significant insulin secretion in mice consecutive to glucose challenge after in vivo maturation of their cells in Encaptra[®]. Another team showed maintained non-fasting glycemia normalization during 6 months after transplanting their cells in alginate microcapsules in diabetic mice.²⁷ On the basis of these data of the literature, additional function studies are currently pursued with MailPan[®] to strengthen the preclinical data with other cell type including stem cells–derived insulin-secreting cells, toward future clinical trials in human.

At the end of function study, cells flushed out from the device showed spontaneous formation of cell clusters inside the MailPan[®]. This known capacity of RIN-m5F once placed on non-adherent support⁶⁵ demonstrated that device materials prevent cell adhesion. In addition, good viability of the retrieved clusters and impairment of glucose tolerance after OGTT following cells retrieval demonstrated a feasible and efficient cell replacement.

Conclusion

This study showed that MailPan[®] is functional in conditions comparable to future clinical trials that we are targeting, with the use of an allogeneic insulin-secreting cell line. Data also highlighted the interest of a pre-vascularization period to guarantee adequate oxygenation to the encapsulated cells at the time of injection. We demonstrated excellent safety of the device, being fully biocompatible, efficiently retaining encapsulated cells and protecting them from the recipient's immune system. In addition, its entry/exit system allowing cell replacement by simple subcutaneous injection would facilitate acceptance of cell therapy by patients.

Acknowledgements

The authors would like to thank the technical team of Center Européen d'Etude du Diabète in Strasbourg for their valuable help in rat islet isolation. Many thanks to Dr André Deratani and Dr Sana Gassara for their expertise in liquid–liquid porometry experiments. We acknowledge Dr Agnès Mechine-Neuville for histological analyses and Dr Elisa Maillard for reviewing this manuscript. Finally, we thank Yoann Valero for his valuable contribution on statistical analyses.

Author contributions

J.M. and S.S. designed the studies. J.M., A.S., A.K., C.T.B., P.G., D.X., and N.T. researched data. J.M., S.S., C.T.B., P.G., D.X., N.T., and B.M. interpreted the data. J.M. and S.S. wrote the manuscript. R.B. reviewed the manuscript. All authors read and approved the manuscript.

Availability of data and material

S.S. is the guarantor of this work and had full access to all of the data in the study and is responsible for the integrity of the data and the accuracy of the data analysis. Datasets generated and analyzed during the current study are available from the corresponding author on reasonable request.

Declaration of conflicting interests

The author(s) declared the following potential conflicts of interest with respect to the research, authorship, and/or publication of this case report: S.S. is founder and stockholder of Defymed S.A.S, sponsor of this work. J.M., A.S., A.K., C.T.B., and R.B. are all employee of Defymed S.A.S.

Ethical approval

All protocols involving animals performed for this study were reviewed by local ethical committees (CREMEAS, Strasbourg, France and CELMEA, Nancy, France) and approved by French Ministry of Research.

Funding

The author(s) disclosed receipt of the following financial support for the research, authorship, and/or publication of this article: This work was funded by the Juvenile Diabetes Research Foundation (JDRF) in the frame of Industry Discovery & Development Partnerships (IDDP), and by Fond Unique Interministériel (FUI), Région Grand Est and Metropole du Grand Nancy through MECABARP collaborative project (16th FUI call for R&D projects).

Informed consent

This study does not involve Human subjects, informed consent is not applicable.

Human rights

Not applicable, this study does not involve any Human subject or Human material.

ORCID iDs

Séverine Sigrist  <https://orcid.org/0000-0002-5766-2596>

Supplemental material

Supplemental material for this article is available online.

References

1. Scharp DW, Lacy PE, Santiago JV, et al. Insulin independence after islet transplantation into type 1 diabetic patient. *Diabetes* 1990; 39: 515–518.
2. Shapiro AM, Lakey JR, Ryan EA, et al. Islet transplantation in seven patients with type 1 diabetes mellitus using a glucocorticoid-free immunosuppressive regimen. *N Engl J Med* 2000; 343(4): 230–238.
3. Ryan EA, Lakey JRT, Rajotte RV, et al. Clinical outcomes and insulin secretion after islet transplantation with the Edmonton protocol. *Diabetes* 2001; 50(4): 710–719.

4. Ahearn AJ, Parekh JR and Posselt AM. Islet transplantation for type 1 diabetes: where are we now. *Expert Rev Clin Immunol* 2015; 11(1): 59–68.
5. Hering BJ, Clarke WR, Bridges ND, et al. Phase 3 trial of transplantation of human islets in type 1 diabetes complicated by severe hypoglycemia. *Diabetes Care* 2016; 39(7): 1230–1240.
6. Plesner A and Verchere CB. Advances and challenges in islet transplantation: islet procurement rates and lessons learned from suboptimal islet transplantation. *J Transplant* 2011; 2011: 979527.
7. Chang CA, Lawrence MC and Naziruddin B. Current issues in allogeneic islet transplantation. *Curr Opin Organ Transplant* 2017; 22: 437–443.
8. Lablanche S, Vantyghem M-C, Kessler L, et al. Islet transplantation versus insulin therapy in patients with type 1 diabetes with severe hypoglycaemia or poorly controlled glycaemia after kidney transplantation (TRIMECO): a multicentre, randomised controlled trial. *Lancet Diabetes Endocrinol* 2018; 6(7): 527–537.
9. Cito M, Pellegrini S, Piemonti L, et al. The potential and challenges of alternative sources of β cells for the cure of type 1 diabetes. *Endocr Connect* 2018; 7: R114–R125.
10. Dadheech N and James Shapiro AM. Human induced pluripotent stem cells in the curative treatment of diabetes and potential impediments ahead. *Adv Exp Med Biol* 2018; 1144: 25–35.
11. Mourad NI and Gianello PR. Xenoislets: porcine pancreatic islets for the treatment of type 1 diabetes. *Curr Opin Organ Transplant* 2017; 22(6): 529–534.
12. Denner J, Tönjes RR, Takeuchi Y, et al. First update of the International Xenotransplantation Association consensus statement on conditions for undertaking clinical trials of porcine islet products in type 1 diabetes—chapter 5: recipient monitoring and response plan for preventing disease trans. *Xenotransplantation* 2016; 23: 53–59.
13. Crossan C, Mourad NI, Smith K, et al. Assessment of porcine endogenous retrovirus transmission across an alginate barrier used for the encapsulation of porcine islets. *Xenotransplantation* 2018; 25(6): e12409.
14. Hentze H, Soong PL, Wang ST, et al. Teratoma formation by human embryonic stem cells: evaluation of essential parameters for future safety studies. *Stem Cell Res* 2009; 2(3): 198–210.
15. Gutierrez-Aranda I, Ramos-Mejia V, Bueno C, et al. Human induced pluripotent stem cells develop teratoma more efficiently and faster than human embryonic stem cells regardless the site of injection. *Stem Cells* 2010; 28(9): 1568–1570.
16. Damjanov I and Andrews PW. Teratomas produced from human pluripotent stem cells xenografted into immunodeficient mice—a histopathology atlas. *Int J Dev Biol* 2016; 60(10–12): 337–419.
17. Scharp DW, Mason NS and Sparks RE. Islet immuno-isolation: the use of hybrid artificial organs to prevent islet tissue rejection. *World J Surg* 1984; 8(2): 221–229.
18. Lin CM and Gill RG. Direct and indirect allograft recognition: pathways dictating graft rejection mechanisms. *Curr Opin Organ Transplant* 2016; 21(1): 40–44.
19. Andres A, Toso C, Morel P, et al. Phylogenetic disparity influences the predominance of direct over indirect pathway of antigen presentation in islet xenotransplantation. *Transplant Proc* 2005; 37(1): 463–465.
20. Rayat GR, Johnson ZA, Beilke JN, et al. The degree of phylogenetic disparity of islet grafts dictates the reliance on indirect CD4 T-cell antigen recognition for rejection. *Diabetes* 2003; 52(6): 1433–1440.
21. Desai T and Shea LD. Advances in islet encapsulation technologies. *Nat Rev Drug Discov* 2016; 16: 338–350.
22. Scharp DW and Marchetti P. Encapsulated islets for diabetes therapy: history, current progress, and critical issues requiring solution. *Adv Drug Deliv Rev* 2014; 67–68: 35–73.
23. Lim F and Sun A. Microencapsulated islets as bioartificial endocrine pancreas. *Science* 1980; 210(4472): 908–910.
24. Hals IK, Rokstad AM, Strand BL, et al. Alginate microencapsulation of human islets does not increase susceptibility to acute hypoxia. *J Diabetes Res* 2013; 2013: 374925.
25. Wang T, Adcock J, Kühtreiber W, et al. Successful allotransplantation of encapsulated islets in pancreatectomized canines for diabetic management without the use of immunosuppression. *Transplantation* 2008; 85: 331–337.
26. Jacobs-Tulleneers-Thevissen D, Bartholomeus K, Suenens K, et al. Human islet cell implants in a nude rat model of diabetes survive better in omentum than in liver with a positive influence of beta cell number and purity. *Diabetologia* 2010; 53(8): 1690–1699.
27. Vegas AJ, Veisoh O, Gürtler M, et al. Long-term glycaemic control using polymer-encapsulated human stem cell-derived beta cells in immune-competent mice. *Nat Med* 2016; 22: 306–311.
28. Harrington S, Williams J, Rawal S, et al. Hyaluronic acid/collagen hydrogel as an alternative to alginate for long-term immunoprotected islet transplantation. *Tissue Eng Part A* 2017; 23: 1088–1099.
29. Yang HK, Ham D-S, Park H-S, et al. Long-term efficacy and biocompatibility of encapsulated islet transplantation with chitosan-coated alginate capsules in mice and canine models of diabetes. *Transplantation* 2016; 100: 334–343.
30. Tuch BE, Keogh GW, Williams LJ, et al. Safety and viability of microencapsulated human islets transplanted into diabetic humans. *Diabetes Care* 2009; 32(10): 1887–1889.
31. Matsumoto S, Abalovich A, Wechsler C, et al. Clinical benefit of islet xenotransplantation for the treatment of type 1 diabetes. *Ebiomedicine* 2016; 12: 255–262.
32. Dufrene D, Goebbels R-M and Gianello P. Alginate macroencapsulation of pig islets allows correction of streptozotocin-induced diabetes in primates up to 6 months without immunosuppression. *Transplantation* 2010; 90: 1054–1062.
33. Barkai U, Weir GC, Colton CK, et al. Enhanced oxygen supply improves islet viability in a new bioartificial pancreas. *Cell Transplant* 2013; 22(8): 1463–1476.
34. Neufeld T, Ludwig B, Barkai U, et al. The efficacy of an immunoisolating membrane system for islet xenotransplantation in minipigs. *PLoS ONE* 2013; 8(8): e70150.
35. Carlsson P-O, Espes D, Sedigh A, et al. Transplantation of macroencapsulated human islets within the bioartificial pancreas β Air to patients with type 1 diabetes mellitus. *Am J Transplant* 2018; 18: 1735–1744.
36. Faleo G, Lee K, Nguyen V, et al. Assessment of immune isolation of allogeneic mouse pancreatic progenitor cells by

- a macroencapsulation device. *Transplantation* 2016; 100: 1211–1218.
37. Pullen LC. Stem cell-derived pancreatic progenitor cells have been transplanted into patients: report from IPITA 2018. *Am J Transpl* 2018; 18: 1581–1582.
 38. Barkai U, Rotem A and de Vos P. Survival of encapsulated islets: more than a membrane story. *World J Transplant* 2016; 6(1): 69–90.
 39. Dionne KE, Colton CK and Yarmush ML. Effect of hypoxia on insulin secretion by isolated rat and canine islets of Langerhans. *Diabetes* 1993; 42(1): 12–21.
 40. Brandhorst D, Brandhorst H, Mullooly N, et al. High seeding density induces local hypoxia and triggers a proinflammatory response in isolated human islets. *Cell Transplant* 2016; 25(8): 1539–1546.
 41. Rodriguez-Brotos A, Bietiger W, Peronet C, et al. Impact of pancreatic rat islet density on cell survival during hypoxia. *J Diabetes Res* 2016; 2016: 3615286.
 42. Jesser C, Kessler L, Lambert A, et al. Pancreatic islet macroencapsulation: a new device for the evaluation of artificial membrane. *Artif Organs* 1996; 20(9): 997–1007.
 43. Barrientos R, Baltrusch S, Sigrist S, et al. Kinetics of insulin secretion from MIN6 pseudoislets after encapsulation in a prototype device of a bioartificial pancreas. *Horm Metab Res* 2009; 41(1): 5–9.
 44. Liu F, Wang M, Wang X, et al. Fabrication and application of nanoporous polymer ion-track membranes. *Nanotechnology* 2019; 30(5): 052001.
 45. Zheng L, Li H, Yu H, et al. “Modified” liquid–liquid displacement porometry and its applications in Pd-based composite membranes. *Membranes* 2018; 8: 29.
 46. Praz GA, Halban PA, Wollheim CB, et al. Regulation of immunoreactive-insulin release from a rat cell line (RINm5F). *Biochem J* 1983; 210(2): 345–352.
 47. Sutton R., Peters M, McShane P, et al. Isolation of rat pancreatic islets by ductal injection of collagenase. *Transplantation* 1986; 42: 689–691.
 48. Pagliuca FW, Millman JR, Gürtler M, et al. Generation of functional human pancreatic β cells in vitro. *Cell* 2014; 159: 428–439.
 49. Rezaei A, Bruin JE, Arora P, et al. Reversal of diabetes with insulin-producing cells derived in vitro from human pluripotent stem cells. *Nat Biotechnol* 2014; 32(11): 1121–1133.
 50. Schulz TC, Young HY, Agulnick AD, et al. A scalable system for production of functional pancreatic progenitors from human embryonic stem cells. *PLoS ONE* 2012; 7(5): e37004.
 51. Randall CL, Kalinin YV, Jamal M, et al. Self-folding immunoprotective cell encapsulation devices. *Nanomedicine* 2011; 7(6): 686–689.
 52. Kobayashi T, Harb G, Rajotte RV, et al. Immune mechanisms associated with the rejection of encapsulated neonatal porcine islet xenografts. *Xenotransplantation* 2006; 13(6): 547–559.
 53. Colton CK. Oxygen supply to encapsulated therapeutic cells. *Adv Drug Deliv Rev* 2014; 67–68: 93–110.
 54. An D, Chiu A, Flanders JA, et al. Designing a retrievable and scalable cell encapsulation device for potential treatment of type 1 diabetes. *Proc Natl Acad Sci U S A* 2018; 115(2): E263–E272.
 55. Bhujbal SV, de Haan B, Niclou SP, et al. A novel multilayer immunoisolating encapsulation system overcoming protrusion of cells. *Sci Rep* 2015; 4: 06856.
 56. Tomei AA, Villa C and Ricordi C. Development of an encapsulated stem cell-based therapy for diabetes. *Expert Opin Biol Ther* 2015; 15(9): 1321–1336.
 57. Carlsson PO, Liss P, Andersson A, et al. Measurements of oxygen tension in native and transplanted rat pancreatic islets. *Diabetes* 1998; 47(7): 1027–1032.
 58. Veriter S, Gianello P, Igarashi Y, et al. Improvement of subcutaneous bioartificial pancreas vascularization and function by coencapsulation of pig islets and mesenchymal stem cells in primates. *Cell Transplant* 2014; 23(11): 1349–1364.
 59. Weaver JD, Headen DM, Hunckler MD, et al. Design of a vascularized synthetic poly(ethylene glycol) macroencapsulation device for islet transplantation. *Biomaterials* 2018; 172: 54–65.
 60. Krishnan R, Arora RP, Alexander M, et al. Noninvasive evaluation of the vascular response to transplantation of alginate encapsulated islets using the dorsal skin-fold model. *Biomaterials* 2014; 35(3): 891–898.
 61. Faleo G, Russ HA, Wisel S, et al. Mitigating ischemic injury of stem cell-derived insulin-producing cells after transplant. *Stem Cell Reports* 2017; 9(3): 807–819.
 62. Skelin M. Pancreatic beta cell lines and their applications in diabetes mellitus research. *ALTEX* 2010; 27(2): 105–113.
 63. Korsgren E and Korsgren O. Glucose effectiveness: the mouse trap in the development of novel β -cell replacement therapies. *Transplantation* 2016; 100: 111–115.
 64. Agulnick AD, Ambruzs DM, Moorman MA, et al. Insulin-producing endocrine cells differentiated in vitro from human embryonic stem cells function in macroencapsulation devices in vivo: insulin-producing endocrine cells from hESCs. *Stem Cells Transl Med* 2015; 4: 1214–1222.
 65. Joo DJ, Kim JY, Lee JJ, et al. Manufacturing of insulin-secreting spheroids with the RIN-5F cell line using a shaking culture method. *Transplant Proc* 2010; 42(10): 4225–4227.